

Dual-Band Filters with Adjustable Bandwidth and Wide Stopband Using CRLH Transmission Line Theory

Chen Li, Minquan Li*, Zhonghui Li, Shuangqing Cao, and Rongxian Bai

Information Materials and Intelligent Sensing Laboratory of Anhui Province, Anhui University, Hefei 230039, China

ABSTRACT: In response to the growing demands of modern communication systems for miniaturized devices, high selectivity, and multi-band characteristics, this paper proposes a design methodology for a dual-band filter based on a planar interdigital structure. Two dual-band filters are developed utilizing transmission zeros and cascading techniques. The filters exhibit high selectivity and wide stopband performance. They are also tunable through parameter adjustments while maintaining a compact form factor. By incorporating composite right/left-handed (CRLH) theory, the proposed filters demonstrate left-handed characteristics. Simulated and experimental results indicate that the designed filters achieve low insertion loss, a wide stopband, and excellent out-of-band rejection within the target frequency bands. Additionally, compared to existing designs in the literature, this approach offers notable advantages in terms of both size and performance. The findings of this study show significant potential for applications in RF and communication systems.

1. INTRODUCTION

The requirements for device miniaturization, wide stopbands, integration, and multi-band capabilities in communication systems are becoming increasingly stringent [1, 2]. As one of the most common components in communication systems, filters must be designed to meet these characteristics.

In 2016, Chen et al. designed a septuple-band filter by leveraging multiple resonators connected in parallel to create multiple coupling paths [3]. This was achieved by parallelizing filters with different frequencies or cascading filtering components to realize multi-frequency filter designs. These filters are characterized by their compact size and high selectivity. In 2017, Shen and colleagues proposed a novel single-mode resonator based on dual-composite right/left-handed (D-CRLH) transmission lines. By cascading two different single-mode resonators, they designed four dual-band filters [4]. In 2018, Q. Yang et al., developed a wide passband filter by combining low-pass filters with open stubs. By increasing the number of open stubs, additional transmission zeros were introduced sequentially, enabling the design of filters with two to seven passbands [5]. The multi-band characteristics were achieved by adding transmission zeros in the stopband region of the filter. In 2020, Liu et al. utilized a balanced dual-mode dual-layer ring resonator to design a dual-band filter [6], achieving controllable transmission zeros and demonstrating excellent selectivity and wide stopband performance. The comprehensive design approach involves obtaining the transfer function of the multi-band filter and using a coupling matrix for simulation. The transfer function is typically derived through the frequency transformation of a normalized low-pass prototype [7]. Left-handed materials, a type of artificial electromagnetic material,

were first proposed by Veselago in 1968 [8]. Due to the right-handed parasitic effects in practical applications of left-handed transmission lines, the concept of composite right/left-handed transmission lines emerged. Microwave devices, such as filters designed using these composite right/left-handed transmission line (CRLH TL), not only maintain excellent filtering performance but also exhibit advantages like compact size and innovative structures. Ref. [9] proposed a method for independently controlling each pair of transmission zeros above and below the passband by leveraging the cross-coupling characteristics of high-order and low-order modes within the substrate integrated waveguide (SIW) cavity. Refs. [10] and [11], based on the proposed superconducting composite right/left-handed (SCRLH) filter, established equivalent lumped element circuit models for differential mode (DM) and common mode (CM), derived the resonant frequencies, and extracted the component values. Theoretical research was conducted on a novel superconducting dual-composite right/left-handed (SD-CRLH) filter, which exhibits wide stopband characteristics, high unloaded quality factor, and compact size.

Unresolved issues in current dual-band filter design: 1) Developing effective methods for designing dual-band filters. 2) Ensuring that the designed filter has high out-of-band suppression. 3) Reducing the size of the filter to address its overly large dimensions. 4) Enhancing the versatility of the filter by enabling resonance points to shift through parameter adjustments.

Innovations in This Paper: 1) We propose a method incorporating transmission zeros and cascading to design two dual-band filters. 2) The designed filters exhibit a wide stopband characteristic. 3) The use of CRLH TL theory enables miniaturization of the filters. 4) The filters that we designed feature adjustable bandwidth capabilities.

* Corresponding author: Minquan Li (AHU411MHz@hotmail.com).

2. ANALYSIS AND DESIGN

2.1. Structure and Parameter Extraction of CRLH Resonator

As shown in Fig. 1, the composite right/left-handed (CRLH) resonator unit proposed by Lai et al. consists of an interdigital structure [12]. It is evident that this structure is composed of interdigital capacitors and short-circuited branches. Here, l_c and W_c represent the length and width of the interdigital structure, while l_s and W_s represent the length and width of the short-circuited branches, and Z represents the input impedance of the interdigital structure.

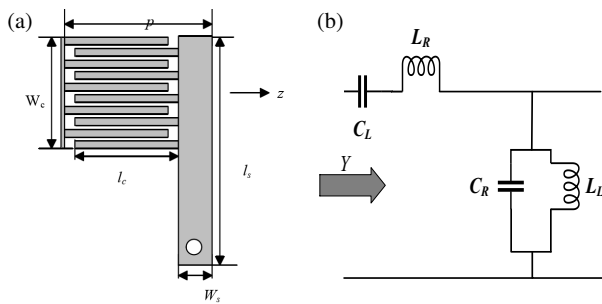


FIGURE 1. (a) CRLH resonator unit. (b) Equivalent circuit diagram of CRLH resonator unit, $W_c = 2.4$ mm, $l_s = 8.0$ mm, $l_c = 5.0$ mm, $P = 6.1$ mm, $W_s = 1$ mm, $L_R = 2.45$ nH, $C_L = 0.68$ pF, $C_R = 0.5$ pF and $L_L = 3.38$ mm.

The input impedance of the short-circuited branch in the resonator unit structure shown in Fig. 1(a) is given as follows:

$$Z = jZ_c \tan(\beta l_s), \quad (1)$$

where Z_c is the characteristic impedance of the microstrip line, and β is the propagation constant at the center frequency. The interdigital inductance value can be estimated from (1) as:

$$L_L \approx \frac{Z_c}{\omega} \tan \beta l_s. \quad (2)$$

The empirical formula for the interdigital capacitance is derived as:

$$C_L \approx (\epsilon_r + 1) l_c [(N - 3) A_1 + A_2] \text{ (pF)}, \quad (3)$$

$$A_1 = 4.409 \tanh \left[0.55 \left(\frac{h}{W_c} \right)^{0.45} \right] * 10^{-6} \text{ (pF}/\mu\text{m)}, \quad (4)$$

$$A_2 = 9.92 \tanh \left[0.52 \left(\frac{h}{W_c} \right)^{0.45} \right]^* 10^{-6} \text{ (pF}/\mu\text{m)}, \quad (5)$$

where h represents the thickness of the dielectric substrate.

As shown in Fig. 1(b), the equivalent circuit diagram of the interdigital structure is presented, where the interdigital unit structure can be equivalently represented as a left-handed capacitance C_L , and the short-circuited branch line is equivalently represented as a left-handed inductance L_L . The value of L_L is determined by the length and width of the short-circuited branch line. These parameters include C_R and L_R , which are parasitic elements generated by the interdigital unit and short-circuited branch.

The input admittance Y of the circuit in Fig. 1(b) is expressed as follows:

$$Y = \frac{(1 - \omega^2/\omega_{se}^2)(1 - \omega^2/\omega_{sh}^2) - \omega^2/\omega_L^2}{j\omega C_L(1 - \omega^2/\omega_{sh}^2)}. \quad (6)$$

When $Y = 0$, resonance occurs in the circuit.

$$(1 - \omega^2/\omega_{se}^2)(1 - \omega^2/\omega_{sh}^2) - \omega^2/\omega_L^2 = 0. \quad (7)$$

The resonance frequency is obtained as:

$$\omega_1 = \frac{a + \sqrt{b}}{2}, \quad \omega_2 = \frac{a - \sqrt{b}}{2}. \quad (8)$$

$$a = \omega_{sh}^2 + \omega_{se}^2 + \omega_L^2, \quad (9)$$

$$b = \omega_{sh}^4 + \omega_{se}^4 + \omega_R^4 - 2\omega_{sh}^2\omega_{se}^2 + 2\omega_R^2\omega_{sh}^2 + 2\omega_R^2\omega_{se}^2. \quad (10)$$

$$W_{se} = \frac{1}{\sqrt{L_L C_L}}, \quad W_{sh} = \frac{1}{\sqrt{L_R C_R}}, \quad W_L = \frac{1}{\sqrt{L_L C_R}}. \quad (11)$$

This design is based on a balanced CRLH TL filter. First, we calculate the frequency points where the input admittance is zero, denoted as ω_1 or ω_2 in (8). Then, using Equations (9) and (10), we can obtain ω_L and ω_R . Finally, the parameter values of C_L , L_L , C_R , and L_R are determined. Next, the design process of a microstrip dual-band filter based on the planar interdigital structure will be introduced in detail. Both filters are designed based on the basic interdigital unit structure mentioned earlier.

2.2. Design of Dual-Band Filters for the n78 and n79 Frequency Bands

In this section, a second-order wide stopband single-band filter operating at 3.5 GHz is first designed using a planar interdigitated structure. A source-load coupling structure is introduced to generate a transmission zero in the stopband, resulting in a second passband at 4.9 GHz. Ultimately, a wide stopband of $2.65f_1$ is achieved, validating the filter's CRLH characteristics through S -parameter inversion [13].



FIGURE 2. Basic topology diagram.

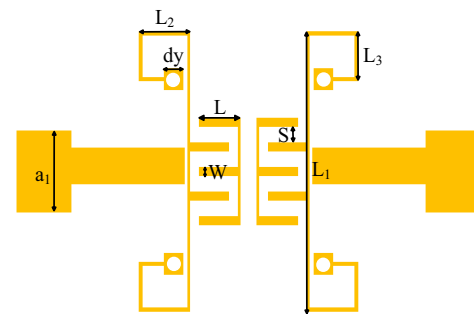


FIGURE 3. Single-band filter structure based on interdigitated structure. $S = 0.85$ mm, $W = 0.5$ mm, $L = 2.2$ mm, $dy = 1.1$ mm, $a_1 = 4.5$ mm, $L_2 = 2.75$ mm, $L_3 = 2.5$ mm and $L_1 = 16.8$ mm.

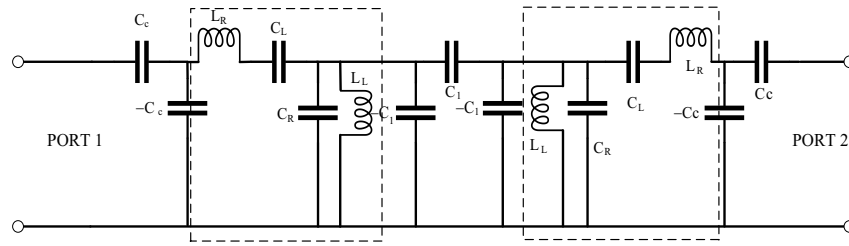


FIGURE 4. Equivalent circuit diagram of the single-band filter structure based on interdigitated structure. $C_c = 1.88$ pF, $L_R = 3.93$ nH, $C_L = 8.49$ pF, $C_R = 2.10$ pF, $C_1 = 0.35$ pF.

As shown in Fig. 2, the basic topology diagram of the designed filter is presented, where $R1$ and $R2$ represent two identical resonators, which are coupled electrically for transmission. S and L represent the source and load, respectively. Based on the overall concept of the topology, the model diagram of the planar interdigital structure is shown in Fig. 3. This structure is designed on a Rogers 5880 dielectric substrate with a dielectric constant of 2.2 and a thickness of 1.575 mm. It is clear that the entire structure is symmetrically distributed, with the ports designed using a coupled feeding method.

The equivalent circuit is shown in Fig. 4, where the dashed box represents the two interdigitated resonator units. The capacitive J transformation is used to represent the electric coupling between the resonators. Similarly, the coupling feed between the input and output ports is also represented by the J transformation. The following analysis will focus on this equivalent circuit diagram.

Firstly, for this two-port network, due to the symmetrical distribution of the circuit, calculating from both ports yields the admittance matrix as follows:

$$[Y] = \begin{bmatrix} \frac{\omega^2 C_1^2 + Y_r}{j\omega^3 C_1^2 C_c + j\omega C_c Y_r^2 + \omega^2 C_c^2 Y_r} & -\frac{Y_b \omega^2 C_1 C_c}{Y_a Y_r + \omega^2 C_1} \\ \frac{Y_b \omega^2 C_1 C_c}{Y_a Y_r + \omega^2 C_1} & \frac{\omega^2 C_1^2 + Y_r}{j\omega^3 C_1^2 C_c + j\omega C_c Y_r^2 + \omega^2 C_c^2 Y_r} \end{bmatrix} \quad (12)$$

$$Y_a = j\omega C_R + \frac{1}{j\omega L_L}, \quad Y_b = j\omega L_R + \frac{1}{j\omega C_L},$$

$$Y_r = Y_a + Y_b. \quad (13)$$

Through the Y matrix, the scattering matrix can be represented as:

$$[S] = \begin{pmatrix} S_{11} & S_{12} \\ S_{21} & S_{22} \end{pmatrix} = \left([U] - [Y]_{filter} \right) \left([U] + [Y]_{filter} \right)^{-1}, \quad (14)$$

where $[U]$ represents the identity matrix.

By substituting the parameters into the above empirical formula and optimizing using HFSS, the specific model parameter values are obtained as: $S = 0.85$ mm, $W = 0.5$ mm, $L = 2.2$ mm, $dy = 1.1$ mm, $a_1 = 4.5$ mm, and $L_2 = 2.75$ mm. Fig. 5 shows the simulation results of the single-band filter. It is apparent that the filter design successfully implements a second-order wide stopband single-band filter operating at 3.5 GHz.

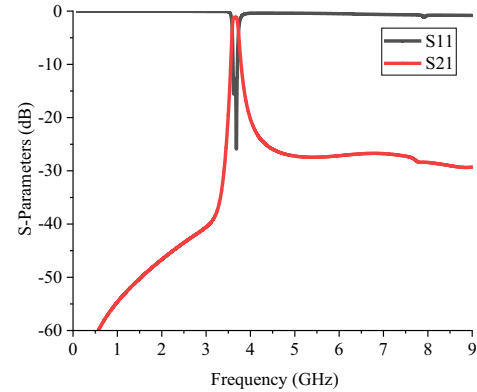


FIGURE 5. Simulation results of the single-band filter.

Based on the above single-band filter structure, a source-load coupling structure is designed to introduce transmission zeros in the stopband, resulting in dual-band filtering characteristics. Fig. 6 shows the improved filter design structure and circuit topology. One can observe that the signal is transmitted through two paths: the main signal path remains unchanged, while an inductive path is added between the source and load. When the transmission signals in the two paths are equal in amplitude and opposite in phase, they add up to create transmission zeros in the stopband. To suppress the spikes of harmonic signals, two symmetrical open-circuit stubs are added, effectively ensuring wide stopband performance. Fig. 7 shows the equivalent circuit diagram of the dual-band filter. In addition to the electric coupling in the main path, an inductive coupling component has also been added.

Below, path1 represents the main signal path, while path2 denotes the source-load coupling path. The two paths are connected in parallel; therefore, the admittance of the filter circuit is equal to the sum of the admittances of each path.

$$[Y] = [Y]_{path1} + [Y]_{path2} \quad (15)$$

$$[Y]_{path1} = \begin{bmatrix} \frac{\omega^2 C_1^2 + Y_r}{j\omega^3 C_1^2 C_c + j\omega C_c Y_r^2 + \omega^2 C_c^2 Y_r} & \\ \frac{Y_b \omega^2 C_1 C_c}{Y_a Y_r + \omega^2 C_1} & \\ -\frac{Y_b \omega^2 C_1 C_c}{Y_a Y_r + \omega^2 C_1} & \\ \frac{\omega^2 C_1^2 + Y_r}{j\omega^3 C_1^2 C_c + j\omega C_c Y_r^2 + \omega^2 C_c^2 Y_r} & \end{bmatrix} \quad (16)$$

$$[Y]_{path2} = \begin{bmatrix} j\omega \frac{L_0^2 - L_1^2}{L_0} & j\omega \frac{L_1}{L_0^2 - L_2^2} \\ j\omega \frac{L_1}{L_1^2 - L_0^2} & j\omega \frac{L_0 - L_1}{L_0} \end{bmatrix} \quad (17)$$

frequency points. This dispersion curve validates the design of the CRLH dual-frequency filter.

2.3. Design of an S-Band Dual-Frequency Filter

A second-order wide stopband single-frequency filter operating at 2 GHz was designed using single-mode CRLH resonators. By paralleling two single-mode CRLH resonators, the filter achieves independently adjustable frequencies, providing filtering and transmission characteristics at S-band frequencies (2 GHz/3.9 GHz). The filter reaches an out-of-band suppression of 15 dB at $2.84f_1$. Equivalent constitutive parameters were extracted using MATLAB to verify the CRLH characteristics of the filter, and the design approach was validated through fabrication and testing.

The following describes a single-frequency filter structure based on Resonator 1 and Resonator 2. This structure is designed using a Rogers 5880 substrate with a thickness of 0.787 mm and a dielectric constant of 2.2. Its planar model is shown in Fig. 10. The entire structure exhibits an up-down symmetric distribution, with two identical resonators achieving electrical coupling by being placed in close proximity. The feed ports consist of $50\ \Omega$ microstrip lines. An equivalent circuit analysis of this filter structure will be conducted below.

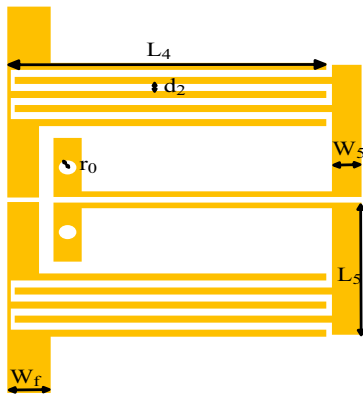


FIGURE 10. Single-frequency filter structure model, $L_4 = 8.95$ mm, $d_2 = 0.25$ mm, $W_5 = 0.84$ mm, $L_5 = 4.7$ mm, $r_0 = 0.25$ mm, $W_f = 1.23$ mm.

Similarly, the J-transformation is used to represent the electrical coupling between the two resonators. The equivalent circuit diagram can be analyzed with reference to the previous discussion, and the specific circuit structure is shown in Fig. 11. The dashed box represents the left-handed circuit, which here refers to the composite left-handed circuit composed of interdigitated capacitors and ground metal vias. The electrical coupling between the two resonators is represented using the J-transformation. A detailed analysis of this equivalent circuit will be provided below. By observing the equivalent circuit, it can be seen that this is a symmetric two-port circuit. The admittance looking into the ports can be expressed as (19).

$$[Y] = \begin{bmatrix} \frac{\omega^2 C_1^2 + Y_r}{\omega^2 C_1^2 + Y_r^2 - Y_r} & \frac{Y_b}{Y_a} \frac{j\omega C_1}{Y_r + \omega^2 C_1} \\ -\frac{Y_b}{Y_a} \frac{j\omega C_1}{Y_r + \omega^2 C_1} & \frac{\omega^2 C_1^2 + Y_r}{\omega^2 C_1^2 + Y_r^2 - Y_r} \end{bmatrix}, \quad (19)$$

$$Y_a = j\omega C_R + \frac{1}{j\omega L_L}, \quad (20)$$

$$Y_b = j\omega L_R + \frac{1}{j\omega C_L}, \quad (21)$$

$$Y_r = Y_a + Y_b. \quad (22)$$

By applying (14), the scattering matrix is obtained. After simulating the equivalent circuit and extracting the parameters, the equivalent lumped component values in the circuit are determined as follows: $L_R = 4.98$ nH, $C_L = 2.34$ pF, $C_R = 3.63$ pF, $L_L = 10.77$ nH, $C_C = 8.48$ pF, $L_c = 18.68$ nH, and $C_1 = 0.15$ pF. Fig. 12 shows the S -parameter simulation results. It can be observed that the filter has a center frequency of 2 GHz, achieving a second-order single-frequency filtering response, with a 20 dB wide stopband characteristic of $2.9f_0$.

As shown in Fig. 13, the basic topology of the filter consists of $R1$, $R2$, $R3$, and $R4$, which represent the interdigitated resonator elements. $R1$ and $R2$, as well as $R3$ and $R4$, are connected through electric coupling. The filter formed by $R1$ and $R2$ operates at a 2 GHz frequency band, while the resonator formed by $R3$ and $R4$ operates at a 3.9 GHz frequency band. The two passbands are independent and can be separately tuned.

Based on the design of the single-frequency filter, the dual-frequency filtering characteristic is achieved next using a cascading method. Fig. 14 shows the structure of a dual-frequency filter composed of four resonators with electrical coupling between each pair. This structure is designed using the same thickness and material as the single-frequency filter's dielectric substrate. This structure is symmetric about the horizontal axis, and the feed ports use $50\ \Omega$ microstrip lines for transmission. The relevant parameters are labeled as shown. It is worth noting that the interdigitated structures are connected by short lines, but it does not affect their individual interdigitated capacitances and short-circuit branches, allowing each to operate independently.

The simulated S -parameter results are shown in Fig. 15. It can be observed that the filter operates in the S-band (2 GHz/3.9 GHz), with insertion losses of 0.33 dB and 0.55 dB for the two passbands, respectively. The dimensions are $0.12\lambda_e \times 0.09\lambda_e$, achieving an out-of-band suppression of 15 dB at $2.84f_1$. This ultimately realizes the design of a miniaturized wide stopband dual-frequency filter. Through equivalent parameter extraction, it can be seen that the permeability and permittivity of the filter change from positive to negative values near 2.2 GHz and 4.0 GHz. When Beta_P is 0, the corresponding resonant frequencies are 2.0 GHz and 3.9 GHz, showing significant changes at these two frequency points, which validates the design of the CRLH dual-frequency filter, as shown in Fig. 16.

Finally, we arrive at the following conclusions. It was determined that L_4 , W_5 , and L_5 primarily affect the transmission characteristics of f_1 , while L_2 , W_1 , and d_1 primarily affect the transmission characteristics of f_2 . Among them, L_2 represents the length of the interdigitated structure corresponding to the C_L value in the left-handed circuit. As L_2 increases, the capacitance increases, and the transmission zero of f_2 shifts to

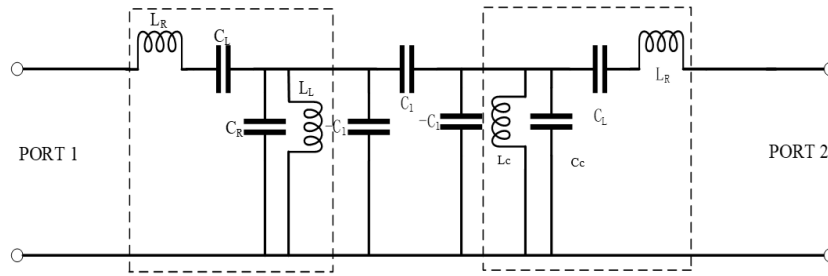


FIGURE 11. Single-frequency filter equivalent circuit.

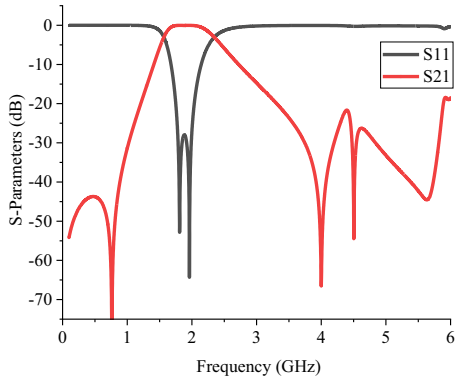


FIGURE 12. Simulation results of the single-frequency filter structure.

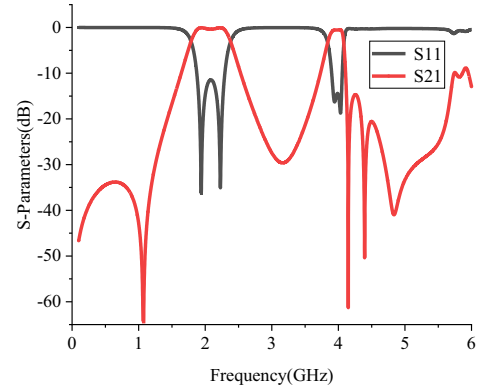


FIGURE 15. Simulation results of the S-band dual-frequency filter.

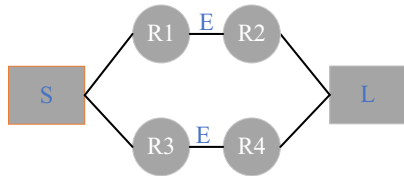


FIGURE 13. Basic topology diagram.

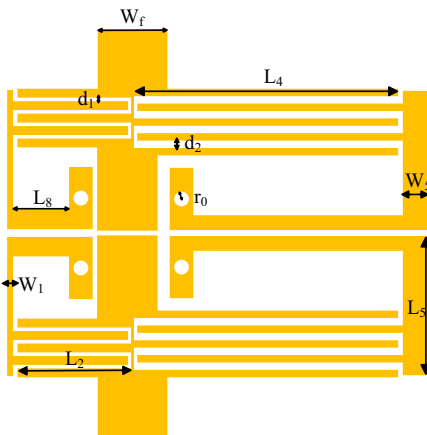


FIGURE 14. Dual-frequency filter structure model, $W_f = 2.36$ mm, $d_1 = 0.12$, $d_2 = 0.25$ mm, $L_4 = 9$ mm, $W_5 = 0.84$ mm, $L_5 = 4.7$ mm, $W_1 = 0.2$ mm, $L_2 = 3.9$ mm, $L_8 = 1.9$ mm, $r_0 = 0.25$ mm.

the left. W_1 represents the width of the interdigitated structure. As W_1 increases, the transmission zero of f_2 shifts to the right, and the bandwidth increases. d_1 represents the gap between the interdigitated structures. As d_1 increases, the capacitance decreases, and f_2 shifts to a higher frequency. Similarly, as L_4

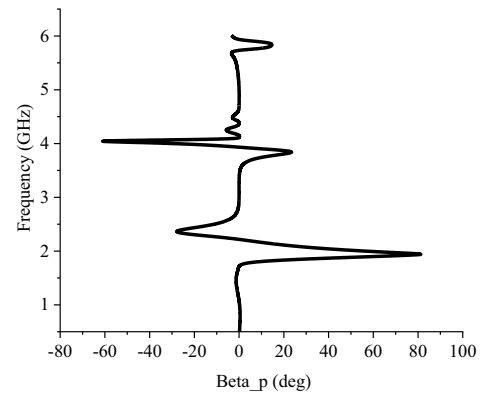


FIGURE 16. S-band filter dispersion curve.

increases, the capacitance of the right-side resonator increases, and the transmission zero of f_1 shifts to the left. As W_5 increases, the transmission zero of f_1 shifts to the right. As L_5 increases, the inductance of the right-side resonator increases, and the transmission zero of f_1 shifts to the left.

3. MEASUREMENT AND ANALYSIS

3.1. Experimental Measurement of the Dual-frequency Filter for the n78 and n79 Bands

The filter model was fabricated and tested, as shown in Fig. 17. Fig. 18 presents the comparison curves of the simulation and test results. From this comparison, it can be observed that the test curve closely matches the simulation curve. However, due to the adjustment of the microstrip line width, which is quite

TABLE 1. Comparison of filter performance with that in the references.

Reference	f_0 (GHz)	IL (dB)	Stopband Width	Size ($\lambda_g \times \lambda_g$)
[14]	10.05/13.70	1.80/1.40	$1.54f_1$ (> 20 dB)	1.27×0.57
[15]	3.50/3.85	1.60/2.82	$1.31f_1$ (> 30 dB)	0.66×0.47
[16]	2.30/2.70	0.90/0.90	$1.60f_1$ (> 30 dB)	0.41×0.20
[17]	3.45/3.55	0.15/0.22	$1.09f_1$ (> 30 dB)	1.02×0.08
This Work	3.43/4.87	2.30/2.20	$2.57f_1$ (> 30 dB)	0.30×0.28

TABLE 2. Comparison of S-band filter performance with references.

Reference	f_0 (GHz)	IL (dB)	Stopband Attenuation	Size ($\lambda_g \times \lambda_g$)
[18]	6.22/8.24	0.86/1.32	$1.77f_1$ (> 20 dB)	0.89×0.41
[19]	8.0/11.4	2.26/3.07	$2.34f_1$ (> 20 dB)	1.93×0.80
[20]	3.6/6.4	1.30/1.80	$2.72f_1$ (> 20 dB)	0.58×0.29
[21]	2.51/5.30	1.41/1.88	$2.39f_1$ (> 20 dB)	0.23×0.45
This Work	2.2/4.1	1.50/1.90	$2.95f_1$ (> 20 dB)	0.10×0.13

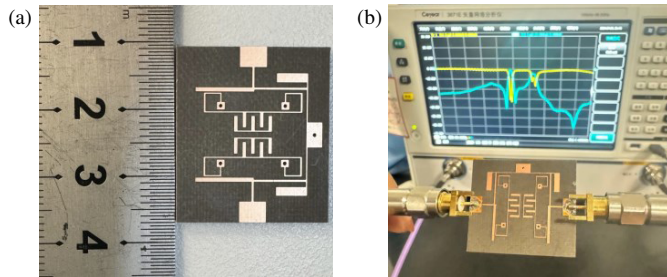


FIGURE 17. Physical image of the filter and test results.

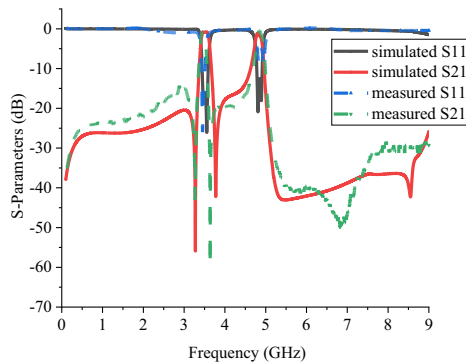


FIGURE 18. Comparison chart of simulation results and measured results of the filter.

narrow (with the narrowest width being only 0.15 mm), the manufacturing process introduced some errors. This caused slight deviations in the measured insertion loss and passband bandwidth. Nevertheless, the comparison shows that the out-of-band rejection is better than the simulation results, achieving a rejection level of 54 dB at 6.9 GHz and 32 dB at 8.0 GHz, with an overall rejection level exceeding 30 dB in the 5–9 GHz range ($2.57f_1$). Table 1 presents a comparison of the performance of the n78 and n79 band filters with those from the literature. Our designed filter demonstrates certain performance advantages.

3.2. Experimental Measurement of the S-Band Dual-Frequency Filter

Figure 19 shows the physical image of the fabricated S-band filter and the test setup using a vector network analyzer in the laboratory. Fig. 20 presents the comparison waveform of the test results and simulation results. The results indicate a rejection level of 21 dB at 4.9 GHz and 34 dB at 6.0 GHz, achiev-

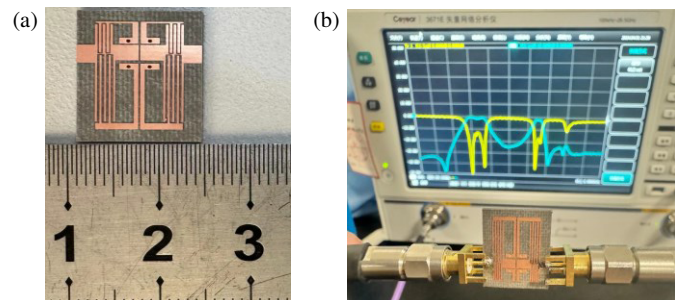


FIGURE 19. Physical image of the S-band filter and test results.

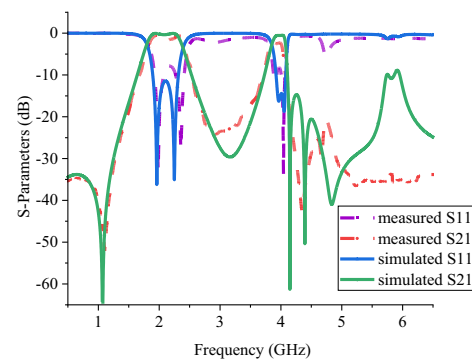


FIGURE 20. Comparison curve of simulation and test results for the S-band filter.

ing an overall rejection level exceeding 20 dB in the 4–6.5 GHz range ($3.25f_1$). Table 2 presents a performance comparison between the S-band filter and various reference filters. The filter designed using the methods outlined in this paper exhibits superior performance.

4. CONCLUSION

This paper proposes a method for designing dual-frequency filters using transmission zeros and cascaded structures, based on planar cross-coupled resonators and composite left/right transmission line theory. The designed filter exhibits low insertion loss, miniaturization, and excellent out-of-band suppression performance. Through the *S*-parameter inversion method, it is demonstrated that both filters exhibit left-handed characteristics. The paper also details how changes in structural parameters lead to variations in the filter's resonance points. Simulation results show good agreement with experimental measurements.

ACKNOWLEDGEMENT

This work was supported in part by Anhui Province Higher Education Science Research Project under Grant 2022AH050070 and in part by the National Natural Science Foundation of China under Grant 62371002.

REFERENCES

- [1] Shen, G., W. Che, W. Feng, Y. Shi, Y. Shen, and F. Xu, "A miniaturized Ka-band bandpass filter using folded hybrid resonators based on monolithic microwave integrated circuit technology," *IEEE Transactions on Circuits and Systems II: Express Briefs*, Vol. 68, No. 6, 1778–1782, Jun. 2021.
- [2] Wang, W., Y. Zheng, and Y. Wu, "Miniaturized single-ended-to-balanced arbitrary four-section coupled-line coupler with inherent impedance matching," *IEEE Transactions on Circuits and Systems II: Express Briefs*, Vol. 67, No. 10, 1929–1933, Oct. 2020.
- [3] Chen, C.-F., S.-F. Chang, and B.-H. Tseng, "Design of compact microstrip sept-band bandpass filter with flexible passband allocation," *IEEE Microwave and Wireless Components Letters*, Vol. 26, No. 5, 346–348, May 2016.
- [4] Shen, G., W. Che, W. Feng, and Q. Xue, "Analytical design of compact dual-band filters using dual composite right-/left-handed resonators," *IEEE Transactions on Microwave Theory and Techniques*, Vol. 65, No. 3, 804–814, Mar. 2017.
- [5] Yang, Q., Y.-C. Jiao, and Z. Zhang, "Compact multiband bandpass filter using low-pass filter combined with open stub-loaded shorted stub," *IEEE Transactions on Microwave Theory and Techniques*, Vol. 66, No. 4, 1926–1938, Apr. 2018.
- [6] Liu, Q., D. Zhang, J. Zhang, D. Zhou, and N. An, "Compact single-and dual-band bandpass filters with controllable transmission zeros using dual-layer dual-mode loop resonators," *IET Microwaves, Antennas & Propagation*, Vol. 14, No. 6, 522–531, 2020.
- [7] Zhang, S. and L. Zhu, "Synthesis design of dual-band bandpass filters with $\lambda/4$ stepped-impedance resonators," *IEEE Transactions on Microwave Theory and Techniques*, Vol. 61, No. 5, 1812–1819, May 2013.
- [8] Veselago, V. G., "The electrodynamics of substances with simultaneously negative values of ϵ and μ ," *Soviet Physics Uspekhi*, Vol. 10, No. 4, 509–514, 1968.
- [9] Chi, P.-L., T.-C. Yeh, and T. Yang, "Compact and high-selectivity SIW multi-channel diplexers and dual-band filters based on the lowest-order dual-mode box-like topology," *IEEE Access*, Vol. 12, 137 870–137 880, 2024.
- [10] Wang, R., H. Liu, and L. Zhu, "A common-mode filter design using superconducting composite right-/left-handed resonators," *IEEE Transactions on Electromagnetic Compatibility*, Vol. 66, No. 1, 169–179, Feb. 2024.
- [11] Wang, R., H. Liu, and L. Zhu, "A VHF-band dual-narrowband HTS filter using superconducting dual-composite right-/left-handed resonators: Design and implementation," *IEEE Transactions on Applied Superconductivity*, Vol. 34, No. 2, 1–10, Mar. 2024.
- [12] Lai, A., T. Itoh, and C. Caloz, "Composite right/left-handed transmission line metamaterials," *IEEE Microw. Mag.*, Vol. 5, No. 3, 34–50, Sep. 2004.
- [13] Numan, A. B. and M. S. Sharawi, "Extraction of material parameters for metamaterials using a full-wave simulator [Education Column]," *IEEE Antennas and Propagation Magazine*, Vol. 55, No. 5, 202–211, 2013.
- [14] Azad, A. R. and A. Mohan, "Substrate integrated waveguide dual-band and wide-stopband bandpass filters," *IEEE Microwave and Wireless Components Letters*, Vol. 28, No. 8, 660–662, Aug. 2018.
- [15] Wu, Y., K. Ma, and Y. Wang, "Coupling matrix design of compact multiband cascaded trisection bandpass filters," *IEEE Transactions on Circuits and Systems II: Express Briefs*, Vol. 69, No. 6, 2762–2766, Jun. 2022.
- [16] Tseng, H.-Y., C.-F. Chen, Y.-H. He, K.-W. Zhou, and R.-Y. Chen, "A microstrip two-state switchable dual-band bandpass filter," in *2020 IEEE Asia-Pacific Microwave Conference (APMC)*, 761–763, Hong Kong, 2020.
- [17] Zhu, L., R. R. Mansour, and M. Yu, "Quasi-elliptic waveguide dual-band bandpass filters," *IEEE Transactions on Microwave Theory and Techniques*, Vol. 67, No. 12, 5029–5037, Dec. 2019.
- [18] Zhang, H., W. Kang, and W. Wu, "Miniaturized dual-band differential filter based on CSRR-loaded dual-mode SIW cavity," *IEEE Microwave and Wireless Components Letters*, Vol. 28, No. 10, 897–899, Oct. 2018.
- [19] Xie, H.-W., K. Zhou, C.-X. Zhou, and W. Wu, "Compact SIW diplexers and dual-band bandpass filter with wide-stopband performances," *IEEE Transactions on Circuits and Systems II: Express Briefs*, Vol. 67, No. 12, 2933–2937, Dec. 2020.
- [20] Zhang, H., W. Kang, and W. Wu, "Miniaturized dual-band SIW filters using E-shaped slotlines with controllable center frequencies," *IEEE Microwave and Wireless Components Letters*, Vol. 28, No. 4, 311–313, Apr. 2018.
- [21] Li, M., C. Chen, and W. Chen, "Miniaturized dual-band filter using dual-capacitively loaded SIW cavities," *IEEE Microwave and Wireless Components Letters*, Vol. 27, No. 4, 344–346, Apr. 2017.